

---

# Correlation effects on electronic transport through dots and wires\*

V. Meden

Institut für Theoretische Physik, Universität Göttingen,  
Friedrich-Hund-Platz 1, D-37077 Göttingen, Germany  
meden@theorie.physik.uni-goettingen.de

**Abstract.** We investigate how two-particle interactions affect the electronic transport through meso- and nanoscopic systems of two different types: quantum dots with local Coulomb correlations and quasi one-dimensional quantum wires of interacting electrons. A recently developed functional renormalization group scheme is used that allows to investigate systems of complex geometry. Considering simple setups we show that the method includes the essential aspects of Luttinger liquid physics (one-dimensional wires) as well as of the physics of local correlations, with the Kondo effect being an important example. For more complex systems of coupled dots and Y-junctions of interacting wires we find surprising new correlation effects.

## 1 Introduction

In recent years the effect of electron correlations on the physics of meso- and nanoscopic systems has attracted growing interest. This led to an increasing overlap of the two communities working on mesoscopic physics and strongly correlated electron systems. In this article we focus on electronic transport properties, in particular the linear response conductance  $G$ . As discussed below two very fundamental correlation effects should be observable in transport through mesoscopic systems of relatively simple structure: (i) the Kondo effect[1] in single quantum dots[2, 3] and (ii) Luttinger liquid (LL) physics in quasi one-dimensional (1d) quantum wires with a single impurity.[4]

The progress in nanostructuring techniques makes it now possible to design more complex geometries such as double- and triple-dot systems[5, 6] and junctions of several quasi 1d wires.[7] In these systems one can expect to find even more interesting correlation physics. In the near future complex setups might be used in conventional devices as well as for quantum information processing which provides a second reason to investigate the role of correlations. The theoretical tools commonly used to study many-body physics in dots and

---

\* In memory of Xavier Barnabé-Thériault, who passed away in a tragic accident on August 15, 2004.

wires are rather specific to simple setups and cannot directly be applied to more complex geometries. Thus, there is need for novel techniques which can properly describe correlations, but are flexible and simple enough such that they can be used to investigate complex systems. In this article, we show that an approximation scheme which is based on the functional renormalization group[8] (fRG) provides such a method. We will first apply it to the two simple setups mentioned above and show that it contains the essential physics. We then proceed and study a system of parallel double-dots and a Y-junction of three 1d quantum wires. In both examples the electron correlations lead to surprising new effects.

To exemplify the importance of correlations we first study transport through a quantum dot with spin degenerate levels. For simplicity we only consider a single level (e.g. described by the single impurity Anderson model[1]) and equal couplings to the left and right lead. The level position can be moved by a gate voltage  $V_g$ . At small  $T$  and for noninteracting dot electrons  $G(V_g)$  shows a Lorentzian resonance of unitary height  $2e^2/h$ . The full width  $2\Gamma$  of the resonance sets an energy scale  $\Gamma$  which is associated with the strength of the tunneling barriers. Including a Coulomb interaction  $U$  between the spin up and down dot electrons the line shape is substantially altered as can be seen from the exact  $T = 0$  Bethe ansatz solution.[9] For increasing  $U/\Gamma$  it is gradually transformed into a box-shaped resonance of unitary height with a plateau of width  $U$  and a sharp decrease of  $G$  to the left and right of it.[2, 3, 10, 11] For gate voltages within the plateau the dot is half-filled implying a local spin-1/2 degree of freedom on the dot. Thus, the Kondo effect[1] leads to resonant transport throughout this so-called Kondo regime. The appearance of the plateau can be understood by studying the characteristics of the one-particle spectral function of the dot. For the present setup  $G(V_g)$  is proportional to the spectral weight at the chemical potential  $\mu$ . [12] For sufficiently large  $U/\Gamma$  the spectral function shows a sharp Kondo resonance (and additional Hubbard bands at higher energies). Its width sets an energy scale—the Kondo temperature  $T_K$ . [10, 1] At half-filling ( $V_g = 0$ ) the peak is located at the chemical potential, but even for gate voltages away from the particle-hole symmetric point it is pinned at  $\mu$  and its height barely changes. This holds for  $-U/2 < V_g < U/2$ , which explains the appearance of the plateau of width  $U$  in the conductance. Experimentally the appearance of Kondo physics in transport through quantum dots was demonstrated clearly.[13, 14]

Although local correlations in a quantum dot (i.e. a zero-dimensional system) already have a strong effect, the system remains a Fermi liquid. However, the low-energy physics of correlated 1d metals (quantum wires) is not described by the Fermi liquid theory. Such systems fall into the LL universality class[4] which is characterized by power-law scaling of a variety of correlation functions and a vanishing quasi-particle weight. For spin-rotational invariant interactions and spinless models, on which we focus here, the exponents of the different correlation functions can be parametrized by a single number, the interaction dependent LL parameter  $K < 1$  (for repulsive interactions;  $K = 1$

in the noninteracting case). Instead of being quasi-particles the low lying excitations of LLs are collective density excitations. This implies that impurities, or more generally inhomogeneities, have a dramatic effect on the physical properties of LLs.[15, 16, 17, 18] In the presence of only a single impurity on asymptotically small energy scales observables behave as if the 1d system was cut in two halves at the position of the impurity, with open boundary conditions at the end points (open chain fixed point).[19, 20, 21] Within a renormalization group approach the impurity increases from weak to strong. For a weak impurity and decreasing energy scale  $s$ —say the temperature  $T$ —the deviation of the linear conductance  $G$  from the impurity-free value first scales as  $(s/s_0)^{2(K-1)}$ , with  $K$  being the scaling dimension of the perfect chain fixed point and  $s_0$  a characteristic energy scale (e.g. the band width). This holds as long as  $|V_{\text{back}}/s_0|^2 (s/s_0)^{2(K-1)} \ll 1$ , with  $V_{\text{back}}$  being a measure for the strength of the  $2k_F$  backscattering of the impurity and  $k_F$  the Fermi momentum. For smaller energy scales or larger bare impurity backscattering this behavior crosses over to another power-law scaling  $G(s) \sim (s/s_0)^{2(1/K-1)}$ , with the scaling dimension of the open chain fixed point  $1/K$ . This scenario was verified within an effective field theoretical model for infinite LLs[19, 20, 21] as well as finite LLs connected to Fermi liquid leads.[22] In the latter case the scaling holds as long as the contacts are modeled to be “perfect”, that is free of any bare and effective single-particle backscattering, and the impurity is placed in the bulk of the interacting quantum wire. Indications of power-law scaling of  $G(T)$  were obtained in experiments on quasi 1d wires, but the results are ambiguous.[23] One reason for this is that experimentally the power-law behavior is restricted to less than one order of magnitude and often only achieved after a somewhat uncontrolled background subtraction on the data.

## 2 The RG method and its application to simple systems

The fRG was recently introduced as a powerful new tool for studying interacting Fermi systems.[8] It provides a systematic way of resumming competing instabilities and goes beyond simple perturbation theory even in problems which are not plagued by infrared divergences.[24] In our applications the dot(s) as well as the interacting quantum wire(s) will be coupled to noninteracting leads as it is the case in systems which can be realized in experiments. Before setting up the fRG scheme we integrate out the leads.[25] In the fRG procedure the noninteracting propagator  $\mathcal{G}_0$  (now including self-energy contributions from the leads) is replaced by a propagator depending on an infrared cutoff  $\Lambda$ . Specifically, we use

$$\mathcal{G}_0^\Lambda(i\omega) = \Theta(|\omega| - \Lambda)\mathcal{G}_0(i\omega) \quad (1)$$

with  $\Lambda$  running from  $\infty$  down to 0. Using  $\mathcal{G}_0^\Lambda$  in the generating functional of the irreducible vertex functions and taking the derivative with respect to  $\Lambda$

one can derive an exact, infinite hierarchy of coupled differential equations for the vertex functions, such as the self-energy and the irreducible 2-particle interaction. In particular, the flow of the self-energy  $\Sigma^A$  (1-particle vertex) is determined by  $\Sigma^A$  itself and the 2-particle vertex  $\Gamma^A$ , while the flow of  $\Gamma^A$  is determined by  $\Sigma^A$ ,  $\Gamma^A$ , and the flowing 3-particle vertex  $\Gamma_3^A$ . The latter could be computed from a flow equation involving the 4-particle vertex, and so on. At the end of the fRG flow  $\Sigma^{A=0}$  is the self-energy  $\Sigma$  of the original, cutoff-free problem we are interested in.[24] A detailed derivation of the fRG flow equations for a general quantum many-body problem which only requires a basic knowledge of the functional integral approach to many-particle physics and the application of the method for a simple toy problem are presented in Ref. [26].

In practical applications the hierarchy of flow equations has to be truncated and  $\Sigma^{A=0}$  only provides an approximation for the exact  $\Sigma$ . As a first approximation we here neglect the 3-particle vertex. The contribution of  $\Gamma_3^A$  to  $\Gamma^A$  is small as long as  $\Gamma^A$  is small, because  $\Gamma_3^A$  is initially (at  $\Lambda = \infty$ ) zero and is generated only from terms of third order in  $\Gamma^A$ . Furthermore,  $\Gamma^A$  stays small for all  $\Lambda$  if the bare interaction is not too large. Below we will clarify the meaning of “not-too-large” in the cases of interest. This approximation leads to a closed set of equations for  $\Gamma^A$  and  $\Sigma^A$ . [27] We here do not give these equations but instead implement a second approximation: the frequency-dependent flow of the renormalized 2-particle vertex  $\Gamma^A$  is replaced by its value at vanishing (external) frequencies, such that  $\Gamma^A$  remains frequency independent. Since the bare interaction is frequency independent, neglecting the frequency dependence leads to errors only at second order for the self-energy, and at third order for the 2-particle vertex at zero frequency. For the approximate flow equations we then obtain

$$\frac{\partial}{\partial \Lambda} \Sigma_{1',1}^A = -\frac{1}{2\pi} \sum_{\omega=\pm\Lambda} \sum_{2,2'} e^{i\omega 0^+} \mathcal{G}_{2,2'}^A(i\omega) \Gamma_{1',2';1,2}^A \quad (2)$$

and

$$\begin{aligned} \frac{\partial}{\partial \Lambda} \Gamma_{1',2';1,2}^A &= \frac{1}{2\pi} \sum_{\omega=\pm\Lambda} \sum_{3,3',4,4'} \left\{ \frac{1}{2} \mathcal{G}_{3,3'}^A(i\omega) \mathcal{G}_{4,4'}^A(-i\omega) \Gamma_{1',2';3,4}^A \Gamma_{3',4';1,2}^A \right. \\ &\quad \left. + \mathcal{G}_{3,3'}^A(i\omega) \mathcal{G}_{4,4'}^A(i\omega) \left[ -\Gamma_{1',4';1,3}^A \Gamma_{3',2';4,2}^A + \Gamma_{2',4';1,3}^A \Gamma_{3',1';4,2}^A \right] \right\}, \quad (3) \end{aligned}$$

where the lower indexes 1, 2, etc. stand for the single-particle quantum numbers and

$$\mathcal{G}^A(i\omega) = [\mathcal{G}_0^{-1}(i\omega) - \Sigma^A]^{-1}. \quad (4)$$

At the initial cutoff  $\Lambda = \infty$  the flowing 2-particle vertex  $\Gamma_{1',2';1,2}^A$  is given by the antisymmetrized interaction and the self-energy by the single-particle terms of the Hamiltonian not included in  $\mathcal{G}_0$  (e.g. impurities).

## 2.1 The single-level quantum dot

Now the set of flow equations can be used to study the two-lead single impurity Anderson model.[1, 28] After integrating out the leads the only relevant single-particle quantum number is the spin  $\sigma$  of the dot electrons. If we take the level energies to be  $\varepsilon_\uparrow = V_g - \mathcal{H}/2$  and  $\varepsilon_\downarrow = V_g + \mathcal{H}/2$ , where  $\mathcal{H}$  denotes a magnetic field which lifts the spin-degeneracy, the projected noninteracting propagator in the so-called wide band limit is given by[1]

$$\mathcal{G}_{0,\sigma}(i\omega) = \frac{1}{i\omega - (V_g + \sigma\mathcal{H}/2) + i\Gamma \operatorname{sgn}(\omega)}, \quad (5)$$

where on the right-hand side  $\sigma = \uparrow = +1$  and  $\sigma = \downarrow = -1$ .

During the fRG flow  $\Sigma^A$  remains frequency independent and  $V_\sigma^A = V_g + \sigma\mathcal{H}/2 + \Sigma_\sigma^A$  can be interpreted as an effective, flowing level position, whose flow equation reads

$$\begin{aligned} \frac{\partial}{\partial \Lambda} V_\sigma^A &= -\frac{U^A}{2\pi} \sum_{\omega=\pm\Lambda} \mathcal{G}_{\bar{\sigma}}^A(i\omega) \\ &= \frac{U^A V_{\bar{\sigma}}^A/\pi}{(\Lambda + \Gamma)^2 + (V_{\bar{\sigma}}^A)^2}, \end{aligned} \quad (6)$$

with the initial condition  $V_\sigma^{A=\infty} = V_g + \sigma\mathcal{H}/2$  and  $\bar{\sigma}$  denoting the complement of  $\sigma$ . The cutoff-dependent propagator  $\mathcal{G}_\sigma^A(i\omega)$  follows from  $\mathcal{G}_{0,\sigma}(i\omega)$  by replacing  $V_g + \sigma\mathcal{H}/2 \rightarrow V_\sigma^A$ . Using symmetries, the flow of the 2-particle vertex can be reduced to a single equation for the effective interaction between spin up and spin down electrons

$$\begin{aligned} \frac{\partial}{\partial \Lambda} U^A &= \frac{(U^A)^2}{2\pi} \sum_{\omega=\pm\Lambda} \left[ \tilde{\mathcal{G}}_\uparrow^A(i\omega) \tilde{\mathcal{G}}_\downarrow^A(-i\omega) + \tilde{\mathcal{G}}_\uparrow^A(i\omega) \tilde{\mathcal{G}}_\downarrow^A(i\omega) \right] \\ &= \frac{2 (U^A)^2 V_\uparrow^A V_\downarrow^A/\pi}{\left[ (\Lambda + \Gamma)^2 + (V_\uparrow^A)^2 \right] \left[ (\Lambda + \Gamma)^2 + (V_\downarrow^A)^2 \right]}, \end{aligned} \quad (7)$$

with  $U^A = \Gamma_{\sigma,\bar{\sigma};\sigma,\bar{\sigma}}^A$  and the initial condition  $U^{A=\infty} = U$ .

Within our approximation the dot spectral function at the end of the fRG flow is given by

$$\rho_\sigma(\omega) = \frac{1}{\pi} \frac{\Gamma}{(\omega - V_\sigma)^2 + \Gamma^2}, \quad (8)$$

with  $V_\sigma = V_\sigma^{A=0}$ , that is a Lorentzian of full width  $2\Gamma$  and height  $1/(\pi\Gamma)$  centered around  $V_\sigma$ . We first consider  $\mathcal{H} = 0$ . Although this spectral function neither shows the narrow Kondo resonance nor the Hubbard bands, for  $U/\Gamma \gg 1$  the pinning of the spectral weight at the chemical potential is included in our approximation. We thus reproduce the line shape of the conductance quantitatively up to very large  $U/\Gamma$ . This is shown in Fig. 1(a) where we plot  $V^{A=0}$  as a function of  $V_g$  (dashed-dotted line) as well as  $G(V_g)$  (dashed

line) for  $U/\Gamma = 4\pi$ . For comparison the exact result for  $G(V_g)$  obtained by Bethe ansatz[9, 11] is shown as the solid line. Neglecting the flow of the two-particle vertex the exponential pinning of spectral weight can even be shown analytically.[28]

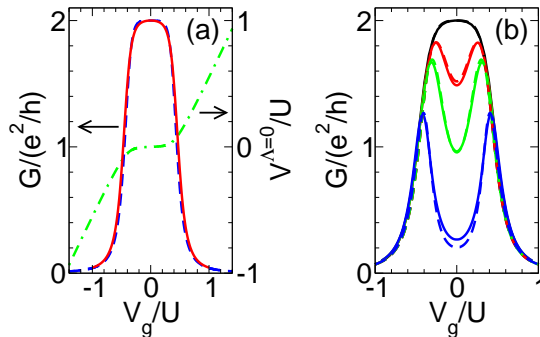


**Fig. 1.** (a) Gate Voltage  $V_g$  dependence of the effective level position  $V^{A=0}$  (dashed-dotted line) and the linear conductance  $G$  (solid line: Bethe ansatz of Ref. [11]; dashed line: fRG) of a single level quantum dot for  $U/\Gamma = 4\pi$ ,  $\mathcal{H} = 0$ . (b)  $G(V_g)$  for  $U/\Gamma = 3\pi$  and  $\mathcal{H} = 0, 0.5T_K, T_K$ , and  $5T_K$ , from top to bottom. Here  $T_K = 0.116\Gamma$ . Solid line: NRG data from Ref. [29]. Dashed line: fRG approximation.

Even without the sharp Kondo resonance in the spectral function, which is usually used to define  $T_K$ , our approximation contains the Kondo temperature. In Fig. 1(b) we show a comparison of fRG data (dashed lines) and high precision numerical renormalization group (NRG) data[29] for  $G(V_g)$  and different  $\mathcal{H}$ . The  $T_K$  given in the caption was obtained from the width of the Kondo resonance at  $V_g = 0$  using NRG. Within NRG at  $\mathcal{H} = T_K$  (third solid curve from top)  $G(V_g = 0) = e^2/h$ . This exemplifies that  $T_K$  can equally be defined as the magnetic field which is necessary to suppress  $G$  down to  $e^2/h$ . This criterion can be used for the fRG data and the excellent agreement of the fRG curves and the NRG results in Fig. 1(b) shows that our approximation (in contrast to other simple approximation schemes) indeed contains  $T_K$ .

We note that using a fRG based truncation scheme in which the full frequency dependence of the 2-particle vertex is kept (leading to a frequency dependent self-energy) it was shown that one can also reproduce the Kondo resonance and Hubbard bands of the spectral function, however with a much higher numerical effort.[24]

## 2.2 A quantum wire with a single impurity

Next we show that the fRG based approximation scheme is also able to produce power-law scaling of the conductance, which is characteristic for inhomogeneous LLs. This requires fairly long chains of interacting electrons—say

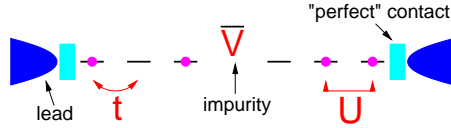


**Fig. 2.** Sketch of the model for an interacting quantum wire with nearest-neighbor hopping  $t$ , nearest-neighbor interaction  $U$ , a local impurity of strength  $V$ , and  $N$  lattice sites. The wire is connected to noninteracting leads by “perfect” contacts.

lattice systems with  $N = 10^4$  sites corresponding to a length in the  $\mu\text{m}$  range. Therefore the fRG flow equations have to be simplified further. For a spinless lattice model of the interacting chain with nearest-neighbor hopping  $t$  and a nearest-neighbor interaction  $U$  (see Fig. 2) we achieve this by parameterizing the  $A$  dependent 2-particle vertex by a flowing nearest-neighbor interaction  $U^A$ . Then  $\Sigma^A$  is a tridiagonal matrix in the real space basis of Wannier states and large systems can be treated.[27] A similar approximation has also been implemented for the (spinful) extended Hubbard model.[30] For the spinless model the LL parameter  $K$  is known exactly from Bethe ansatz.[31] Besides  $U$  it also depends on the filling  $n$ . To compute  $G(T)$  one has to generalize the fRG to  $T > 0$ . This is described in Refs. [25] and [30]. We obtain the conductance from the one-particle Green function (and thus the self-energy) using a generalized Landauer-Büttiker relation.[25] Within our approximation current vertex corrections vanish (because  $\Sigma^{A=0}$  is real) and using this relation does not require any additional approximations.[25] As we are only interested in the effect of a single impurity we model the contacts between the leads and the interacting wire to be “perfect”, that means for  $V = 0$  (see Fig. 2) the  $T = 0$  conductance through the wire is  $e^2/h$ . This requires that the interaction is turned on and off smoothly close to the contacts.[25]

The power-law scaling of  $G(T)$  close to the perfect and open chain fixed points can very elegantly be shown in a single plot using a one-parameter scaling ansatz. Plotting  $G(T)$  as a function of  $T/T_0$ , with an appropriately chosen nonuniversal scale  $T_0(U, n, V)$ , all data obtained for different  $V$ ,  $U$ , and  $n$ —with the restriction that  $K(U, n)$  is fixed—collapse on a single  $K$  dependent curve.[19, 21] This is shown in Fig. 3. The open symbols were obtained for  $n = 1/2$ ,  $U = 0.5$  while the filled ones were computed for  $n = 1/4$ ,  $U = 0.851$ , both parameter sets leading to  $K = 0.85$ . Different symbols stand for different  $V$ . For convenience  $(T/T_0)^{K-1}$  is chosen as the  $x$ -axis such that  $G/(e^2/h)$  for  $x \ll 1$  scales as  $1 - x^2$  and for  $x \gg 1$  as  $x^{-2/K}$ . Within our approximation the scaling exponents are correct to leading order in  $U$ . [27, 25, 30] During the flow the self-energy remains frequency independent and  $\Sigma^{A=0}$  can be interpreted as an effective impurity potential. Scattering off the spatially long-ranged oscillations of the self-energy generated during the fRG flow leads to the observed power-law behavior.[27, 25]

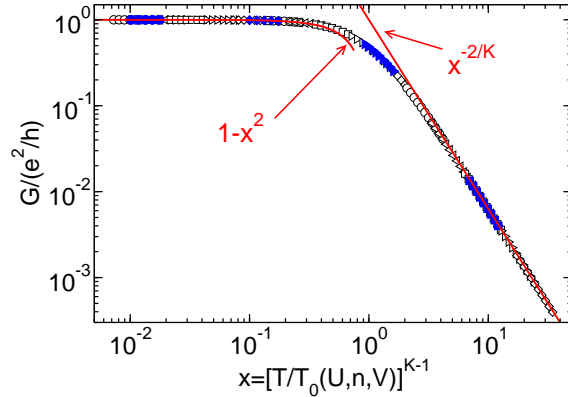


**Fig. 3.** One-parameter scaling of  $G(T)$  for a quantum wire with  $N = 10^4$  lattice sites and a single impurity. For details see the text.

We note that in the limits of weak and strong impurities the scaling can be shown analytically with our fRG scheme.[32] Up to now the fRG is the only method which allows to study the entire crossover from weak to strong impurities for microscopic lattice models. Studying such models is important as similar to experimental systems, they contain energy scales that set upper and lower bounds for scaling. They are absent if field theoretical models are used.

### 3 Correlation effects in more complex geometries

After showing that our method contains the essential physics in the case of locally correlated systems as well as for inhomogeneous LLs we proceed and study more complex setups.

#### 3.1 Novel resonances in a parallel double-dot system

As a first example we consider a parallel single-level double-dot system as sketched in Fig. 4(a). The dots are coupled to common leads by tunneling barriers and the electrons interact by an inter-dot interaction  $U$ . The ring geometry is pierced by a magnetic flux  $\phi$ . We here neglect the spin and thus suppress the spin Kondo effect. Experimentally, the contribution of spin physics may be excluded by applying a strong magnetic field. We focus on temperature  $T = 0$ . For this setup the flow equations (2) and (3) can directly be applied.  $G$  is computed from a generalized Landauer-Büttiker relation.[28]

Fig. 4(b) shows the evolution of  $G(V_g)$  for degenerate levels  $\varepsilon_j = V_g$ , generic parameters[33]  $\Gamma_j^l$ ,  $\phi$ , and increasing  $U$ . At  $U = 0$ ,  $G(V_g)$  is a Lorentzian at large  $|V_g|$ , while it shows a dip at  $V_g = 0$ . With increasing

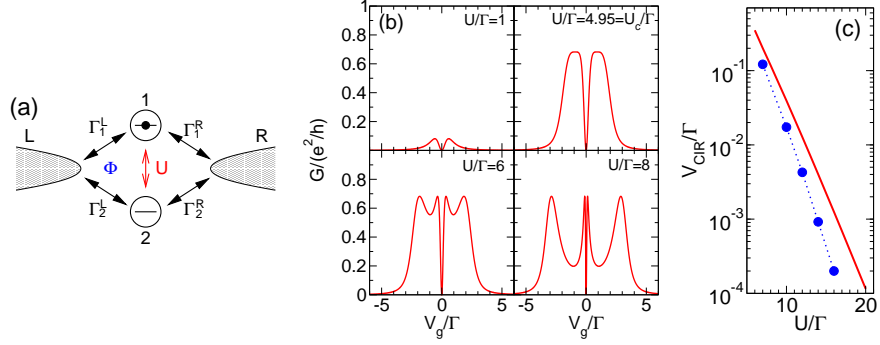


**Fig. 4.** (a) Sketch of the double-dot setup. (b) Generic results for  $G(V_g)/(e^2/h)$  at different  $U$  obtained from the fRG with  $\Gamma_1^L = 0.27\Gamma$ ,  $\Gamma_1^R = 0.33\Gamma$ ,  $\Gamma_2^L = 0.16\Gamma$ ,  $\Gamma_2^R = 0.24\Gamma$ , and  $\phi = \pi$ . The two novel correlation induced resonances are visible in the lower panels (large  $U$ ), near  $V_g = 0$ . (c)  $U$  dependence of the position  $V_{\text{CIR}}$  of the novel resonances (line: fRG; circles: NRG).

$U$  the height of the two peaks resulting from the dip at  $V_g = 0$  increases and the maximum flattens. At a critical  $U = U_c(\{\Gamma_j^l\}, \phi)$  each peak splits into two. For the present example the fRG approximation is  $U_c/\Gamma \approx 4.69$ , with  $\Gamma$  being the sum over all  $\Gamma_j^l$ . Further increasing  $U$  the two outer most peaks move towards larger  $|V_g|$  and become the Coulomb blockade peaks located at  $V_g \approx \pm U/2$ . The other two peaks at  $\pm V_{\text{CIR}}$ , where  $V_{\text{CIR}} > 0$  decreases with increasing  $U$ , are novel resonances following from the interplay of quantum interference and correlations. For  $U > U_c$  the height of all four peaks is equal and does not change with  $U$ . Note that in contrast to Ref. [33] here the flow of the 2-particle vertex is included which leads to improved results. The above scenario was confirmed using NRG.[33] Furthermore, the appearance of the novel resonances is robust: It appears for almost arbitrary combinations of the four tunnel couplings and the magnetic flux, also remains visible for a small detuning of the dot level energies,[33] and small temperatures. In Fig. 4(c) we show the dependence of  $V_{\text{CIR}}$  on  $U$  obtained from fRG (line) and NRG (circles) on a linear-log scale. Both curves follow a straight line which shows that

$$V_{\text{CIR}}/\Gamma \propto \exp[-C(\{\Gamma_j^l\}, \phi) U/\Gamma], \quad (9)$$

with  $C > 0$ . The fRG apparently underestimates  $C$ . Within the fRG for a certain class of  $\{\Gamma_j^l\}, \phi$  the appearance of an energy scale depending exponentially on  $U/\Gamma$  can be shown analytically.[33] We note that the above correlation effect is unrelated to spin and orbital Kondo physics.

Double-dot geometries that could form the basis to verify the above predictions have been experimentally realized in Ref. [5].

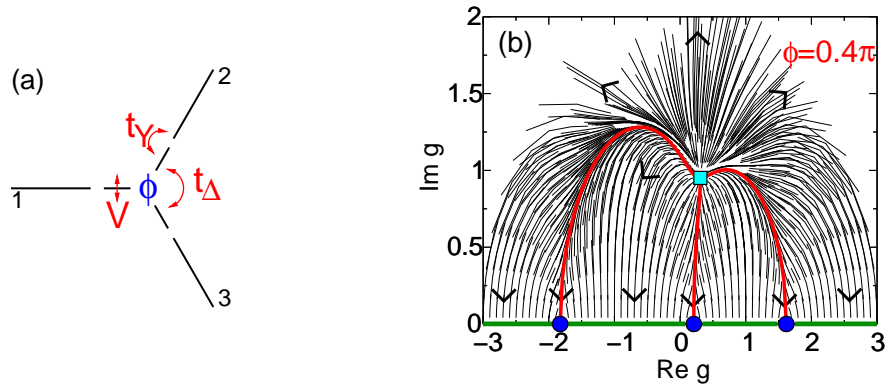


**Fig. 5.** (a) Setup of the Y-junction of three interacting quantum wires. (b)  $U > 0$  fRG flow within the complex  $g$  plane. For each point in the  $g$  plane the conductance follows using Eq. (10). The symbols indicate fixed points. The condition  $\text{Im } g = 0$  defines a line of fixed points. For further details see the text.

### 3.2 Novel fixed points in a Y-junction of three quantum wires

As a second example for the application of the fRG to more complex geometries we study the conductance through a Y-junction of interacting quantum wires. The three wires are assumed to be equal and described by the model of spinless fermions with nearest-neighbor hopping  $t$  and nearest-neighbor interaction  $U$  as already used above. Each wire is connected to noninteracting leads by “perfect” contacts. The junction is assumed to be symmetric and characterized by three parameters  $t_Y$ ,  $t_\Delta$ , and  $V$  as sketched in Fig. 5(a). The ring structure is furthermore pierced by a magnetic flux  $\phi$  and for  $\phi \neq n\pi$ , with an integer  $n$ , time-reversal symmetry is broken. For generic junction parameters in the non-interacting case this leads to an asymmetry of the conductance from wire  $\nu$  to wire  $\nu'$  (with  $\nu, \nu' = 1, 2, 3$ ) and vice versa  $G_{\nu, \nu'} \neq G_{\nu', \nu}$  and the breaking of time-reversal symmetry is indicated by the conductance. This can be seen using single-particle scattering theory.  $G_{\nu', \nu}$  can be expressed in terms of the single complex and junction parameter dependent number  $g = (-V - t_Y^2 \tilde{\mathcal{G}}_{1,1})/|t_\Delta|$  as

$$G_{\nu, \nu'} = \frac{4(\text{Im } g)^2 |e^{-i\phi} - g|^2}{|g^3 - 3g + 2 \cos \phi|^2}, \quad (10)$$

with  $\nu, \nu'$  in cyclic order.[34]  $G_{\nu', \nu}$  follows by replacing  $\phi \rightarrow -\phi$ . Here  $\tilde{\mathcal{G}}$  denotes the (wire index independent) single particle Green function of one of the semi-infinite wires obtained after setting  $t_Y = 0$  and taking the energy  $\varepsilon + i0$  with  $\varepsilon \rightarrow 0$ . The index 1, 1 stands for its diagonal matrix element taken at the first site. At  $U = 0$  it is given by  $\tilde{\mathcal{G}}_{1,1} = i/t$ . [25]

At  $T = 0$  Eq. (10) also holds for  $U > 0$ . In this case  $\tilde{\mathcal{G}}_{1,1}(\Sigma)$  becomes self-energy and thus  $U$  dependent. As for the single interacting wire with one impurity  $\Sigma$  can approximately be computed using the fRG. As scaling variable we this time use an energy scale  $\delta_N = \pi v_F/N$ , with  $v_F$  being the  $U = 0$  Fermi velocity, set by the length of the three interacting wires. As  $\Sigma^{\Lambda=0}$  becomes  $\delta_N$  dependent, also  $g$  and thus  $G_{\nu,\nu'}$  will depend on the length of the interacting wires. Increasing  $N$  (that is lowering the infrared cutoff  $\delta_N$ ) for fixed  $U, \phi \neq n\pi, t_Y, t_\Delta, V$  then leads to a flow in the complex  $g$  plane and  $G_{\nu,\nu'}$  changes according to Eq. (10). The flow for  $U = 1$  and  $\phi = 0.4\pi$  is shown in Fig. 5(b) for a variety of different  $t_Y, t_\Delta, V$ . Each line stands for a fixed set of the junction parameters and varying  $\delta_N$ . The direction of the flow is indicated by the arrows.

The square indicates a fixed point at which the asymmetry is maximal, that is  $G_{1,2} = e^2/h$  and  $G_{2,1} = 0$ . For  $U > 0$  it is unstable.[35, 34] For generic junction parameters the flow is directed towards the line of fixed points defined by the  $\text{Im } g = 0$  line. As is apparent from Eq. (10) on this line and for generic  $\text{Re } g$ , both  $G_{1,2}$  and  $G_{2,1}$  vanish. This line of fixed points is the analogue of the open chain fixed point obtained for one impurity in a single wire. Analyzing the scaling close to the line of fixed points in more detail we find that for  $\delta_N \rightarrow 0$ ,  $|G_{1,2} - G_{2,1}|/(G_{1,2} + G_{2,1}) \rightarrow 0$ , i.e.  $G_{1,2}$  and  $G_{2,1}$  become equal faster than they go to zero. Even more surprising behavior is found if the bare parameters are tuned such that the flow starts on the thick line. In that case it leads to one of the three fixed points indicated by the circles. On these fixed points we find  $G_{1,2} = G_{2,1} = (4/9)(e^2/h)$ , which is the conductance maximally allowed by the unitarity of the scattering matrix for a symmetric Y-junction of noninteracting wires. Combined, these two observations show that due to the interaction on very low energy scales (i.e. for long interacting wires and at low temperatures) the conductance no longer indicates a broken time-reversal symmetry. In that sense the electron correlations restore the time-reversal symmetry.[34]

Associated to the novel  $(4/9)(e^2/h)$  fixed points is a novel scaling dimension that should show up in e.g. the finite temperature corrections of  $G$  with respect to the fixed point conductance.[34]

## 4 Summary

In the present article we have shown that electron correlations in nano- and mesoscopic systems can lead to a variety of surprising effects. While for simple geometries established methods are available to investigate important aspects of the many-body problem, they cannot directly be applied to more complex setups, such as systems of locally correlated quantum dots and junctions of interacting quantum wires. To investigate such systems, which in the near future will shift towards the focus of experimental activities, we introduced a reliable, simple to implement, and numerically very fast approximation scheme

which is based on the functional renormalization group. In certain limiting cases it can also be used to obtain analytical results.

The author would like to thank T. Costi and J. von Delft for providing their NRG and Bethe ansatz data, S. Andergassen, T. Enss, C. Karrasch, F. Marquardt, W. Metzner, U. Schollwöck, K. Schönhammer, and A. Sedeki for collaboration on the issues presented, and P. Wächter for useful comments on the manuscript. This work was supported by the Deutsche Forschungsgemeinschaft (SFB 602).

## References

1. A.C. Hewson, *The Kondo Problem to Heavy Fermions*, (Cambridge University Press, Cambridge, UK, 1993)
2. L. Glazman and M. Raikh, *JETP Lett.* **47**, 452 (1988)
3. T. Ng and P. Lee, *Phys. Rev. Lett.* **61**, 1768 (1988)
4. For a review see K. Schönhammer in *Interacting Electrons in Low Dimensions*, Ed.: D. Baeriswyl, Kluwer Academic Publishers (2005)
5. A. W. Holleitner *et al.*, *Phys. Rev. Lett.* **87**, 256802 (2001); *Science* **297**, 70 (2002)
6. N.J. Craig *et al.*, *Science* **304**, 565 (2004)
7. M. Terrones *et al.*, *Phys. Rev. Lett.* **89**, 075505 (2002)
8. M. Salmhofer, *Renormalization*, (Springer, Berlin, 1998)
9. A.M. Tsvelik and P.B. Wiegmann, *Adv. Phys.* **32**, 453 (1983)
10. T.A. Costi, A.C. Hewson, and V. Zlatic, *J. Phys.: Condens. Matter* **6**, 2519 (1994)
11. U. Gerland, J. von Delft, T.A. Costi, and Y. Oreg, *Phys. Rev. Lett.* **84**, 3710 (2000)
12. Y. Meir and N.S. Wingreen, *Phys. Rev. Lett.* **68**, 2512 (1992)
13. D. Goldhaber-Gordon *et al.*, *Nature* **391**, 156 (1998)
14. W. van der Wiel *et al.*, *Science* **289**, 2105 (2000)
15. A. Luther and I. Peschel, *Phys. Rev. B* **9**, 2911 (1974)
16. D.C. Mattis, *J. Math. Phys.* **15**, 609 (1974)
17. W. Apel and T.M. Rice, *Phys. Rev. B* **26**, 7063 (1982)
18. T. Giamarchi and H.J. Schulz, *Phys. Rev. B* **37**, 325 (1988)
19. C.L. Kane and M.P.A. Fisher, *Phys. Rev. Lett.* **68**, 1220 (1992); *Phys. Rev. B* **46**, 15233 (1992)
20. A. Furusaki and N. Nagaosa, *Phys. Rev. B* **47**, 4631 (1993)
21. P. Fendley, A.W.W. Ludwig, and H. Saleur, *Phys. Rev. Lett.* **74**, 3005 (1995)
22. A. Furusaki and N. Nagaosa, *Phys. Rev. B* **54**, R5239 (1996)
23. M. Bockrath *et al.*, *Nature* **397**, 598 (1999); Z. Yao, H. Postma, L. Balents, and C. Dekker, *Nature* **402**, 273 (1999); O. Auslaender *et al.*, *Phys. Rev. Lett.* **84**, 1764 (2000); R. de Picciotto *et al.*, *Nature* **411**, 51 (2001)
24. R. Hedden, V. Meden, Th. Pruschke, and K. Schönhammer, *J. Phys.: Condens. Matter* **16**, 5279 (2004)
25. T. Enss *et al.*, *Phys. Rev. B* **71**, 155401 (2005)
26. V. Meden, lecture notes on the “Functional renormalization group”, <http://www.theorie.physik.uni-goettingen.de/~meden/funRG/>

27. S. Andergassen *et al.*, Phys. Rev. B **70**, 075102 (2004)
28. C. Karrasch, T. Enss, and V. Meden, cond-mat/0603510
29. T.A. Costi, Phys. Rev. B **64**, 241310(R) (2001)
30. S. Andergassen *et al.*, Phys. Rev. B **73**, 045125 (2006)
31. F.D.M. Haldane, Phys. Rev. Lett. **45**, 1358 (1980)
32. V. Meden, W. Metzner, U. Schollwöck, and K. Schönhammer, J. of Low Temp. Physics **126**, 1147 (2002)
33. V. Meden and F. Marquardt, Phys. Rev. Lett. **96**, 146801 (2006)
34. X. Barnabé-Thériault, A. Sedeki, V. Meden, and K. Schönhammer, Phys. Rev. Lett. **94**, 136405 (2005)
35. C. Chamon, M. Oshikawa, and I. Affleck, Phys. Rev. Lett. **91**, 206403 (2003)